Analyses of the anisotropic flow in Pb-Pb collisions at $\sqrt{s_{NN}}$ =2.76 TeV

Tommie Koot
Studentnumber: 3471519
Institute for Subatomic Physics
Universiteit Utrecht

Supervised by:
Dhr. prof. dr. RJM Snellings
Dhr. dr. AF Dobrin

June 14, 2013

Abstract

Heavy-ion collisions are used to study the hot and dense matter that might have existed just after the Big Bang. This so called quark gluon plasma is one of the subjects that is studied in sub-atomic particle physics. The purpose of this research is to study the anisotropic flow. The anisotropic flow is an observable that can give more information about the properties of the quark gluon plasma. In this research data collected in November and December by the ALICE detector during the Pb-Pb run is used. The calculations have been done for a transverse momentum range $0.2 < p_T < 6$ GeV/c, within the pseudorapidity interval (-0.8,0.8). The method used in this analysis is the two particle correlation technique. In this research the charged particle elliptic and triangular flow will be discussed in great detail, as will their systematic errors. Some background information is also provided in the first chapter.

Contents

Chapter 1

Heavy Ion Collisions

Heavy-ion physics is focused on studying the hot and dense matter created in heavy-ion collisions. Lorentz contracted ions collide with each other at relativistic speeds to create these circumstances. Because of their relativistic speed, the heavy ions approach each other as flat disks. In case of a collision, an impact parameter (b) is determined. The impact parameter (b) is defined as the transverse distance between the centre of the two nuclei. This parameter can be used to quantify the overlapping region between the two colliding nuclei. This impact parameter cannot be determined experimentally, instead another parameter is used to quantify the overlapping region. The centrality can be defined as the degree of overlap in a collision. The centrality can be between 0 and 100%. In this research a centrality of 0% means that the collision was head on. The higher the percentage the more peripheral the collision is. The centrality can be calculated with the impact parameter, but because the impact parameter cannot be measured directly, a Glauber model is used to estimate the number of participants and the number of collisions. Inside the overlapping region between the nuclei the nucleons interact with each other, which creates a hot and dense volume that expands rapidly. At the outside of the overlapping region the particles continue without interacting. They just pass by with the same momentum they had before, these non interacting nucleons are referred to as spectator nucleons. The interacting nucleons are referred to as participant nucleons.

1.1 Quark gluon plasma

According to the Big Bang theory, only a fraction of a second after the Big Bang, the universe was so dense and hot that no nuclei could be formed. What did exist was the Quark Gluon Plasma (QGP). Quarks are elementary particles that are the fundamental building blocks of matter. They have an electric charge, colour charge, spin and mass. The gluons are the particles that transfer the strong force between the quarks. Just like the quarks they also have a colour charge. Inside the plasma the quarks and gluons are moving freely [7]. As the universe expanded quarks and gluons combined into nucleons as the interaction between quarks became stronger as they got further apart, which caused the quarks and gluons to disappear as single particles [1]. The reason for this is that at high

temperatures and short distances the quarks exchange less gluons, but as they separate further away more gluons are exchanged between the quarks which increases the attraction between them. This is what is called their asymptotic freedom. As a result there are no free quarks found at low temperature and large distances. At the universe's current temperature, there are only a few places left where the QGP might exists. One of the options is in very heavy neutron stars, where the temperature and density are high enough to break up the hadrons [10].

There is a lot of energy needed to recreate this kind of temperature and density in an accelerator. There are several accelerators that are used to study the QGP. The first one, the Large Hadron Collider (LHC) is currently, with an energy of 2.76 TeV per nuclei in the centre of mass, the accelerator with the highest energy per nuclei. Not only in Europe are they studying the QGP, in the United States they are using the Relativistic Heavy Ion Collider (RHIC) to collide gold nuclei at 200 GeV. Different observables are used to study the properties and evolution of heavy-ion collisions [14]:

- Strange quarks production
- Direct measurements of fluctuation in the charge distribution at collisions.
- Jet quenching.
- The anisotropic flow

In this thesis, the focus will be on the anisotropic flow.

1.2 Anisotropic flow

The anisotropic azimuthal distribution is a much used variable in particle physics. Anisotropies in particle momentum distributions relative to the reaction plane have been used for the past decades and it is referred to as anisotropic collective flow. With the experimental discovery of elliptic flow it got a renewed attention. Because the asymmetric momentum distribution is getting less anisotropic over time, it was concluded that the anisotropy can only be formed in the early part of the collision and therefore it is only sensitive to the early stage of the collision [16].

Anisotropic flow is used to study the thermodynamic properties as well as the equation of state of the hot and dense matter after the collision. At high transverse momentum it can also be used to study the energy loss. In order for the anisotropic flow to develop fully, the longitudinal size of the nuclei has to be negligible. For this the ions must reach high relativistic velocities. If there is no re-scattering, the anisotropic flow should be zero. At low densities this means that the anisotropic flow is proportional to the particle density. For a completely symmetric azimuthal angle distribution, the anisotropic flow is also zero. Small fluctuations in the azimuthal angle of the particles in combination with the interactions between the particles will create the anisotropic distribution.

Two nuclei that collide in heavy ion collisions are almost completely flat disks because of the relativistic effects. Non central collision will therefore have an almond like shape as can be seen in Figure 1.1.

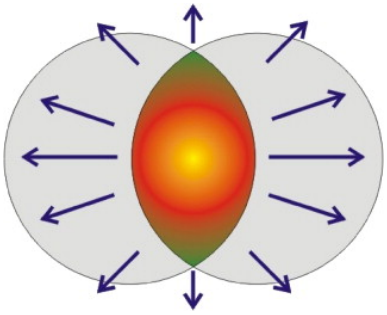

Figure 1.1: The overlapping region of a collision. In this picture, one beam is coming out of the paper, while the other one is travelling into it. [9]

The almond shape creates a pressure difference within the overlapping region, which results in an asymmetric expansion. The pressure gradient causes more particles to move to the flanks of the almond shape than to the top of it.

1.2.1 Methods for calculating anisotropic flow

There are two planes that are used to describe collisions: the reaction plane and the participant plane. The reaction plane is spanned by the vector of the impact parameter and the beam direction (z axis), while the participant plane is made by the interacting particles and the beam direction. The difference between the planes can be seen below.

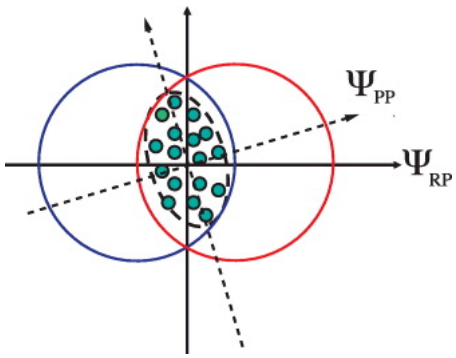

Figure 1.2: The reaction plane and participant plane relative to each other. [11]

Since the azimuthal distribution of particles is not isotropic in the reaction plane, it is expanded into a Fourier series [15].

$$E\frac{d^3N}{d^3p} = \frac{1}{2\pi}\frac{d^2N}{p_T dp_T dy}(1 + \sum_{n-1}^{\infty} 2v_n \cos(n(\phi - \Psi_{RP}))), \tag{1.1}$$

where the $v_n = \langle\cos(n(\phi_i - \Psi_{RP}))\rangle$ are used to express the event anisotropy. The ϕ_i is the azimuthal angle for each individual track per event. The v_n are the flow coefficients, v_1 is the directed flow, v_2 is the elliptic flow and v_3 is the triangular flow.

The flow coefficients can be calculated with use of the two or multi particle correlations. The correlations are not only caused by the anisotropic flow but also by non-flow origins such as jets, resonance decay and momentum conservation. Most of the non-flow effects are for few particle correlations. Higher multiplicities therefore reduce the contribution of the non-flow correlations. The correlation with the addition of non-flow effects can be written down as:

$$\langle \cos(n(\phi_i - \phi_j)) \rangle = \langle v_n^2 \rangle + \delta_n \tag{1.2}$$

The anisotropic flow differs from event to event. These so called flow fluctuations can have many sources. An important source of this is the initial geometry of the collision. The geometry fluctuates because the interactions between the colliding nuclei have a random nature. These fluctuations in the geometry are the reason why there is a difference between the reaction plane and the participant plane. The result from these fluctuations is that the flow coefficients of the reaction plane and the participant plane have different values, in the way that $v_{RP} < v_{PP}$. If the region of interaction would be a perfect almond shape, the odd harmonics (v_3,v_5..) would all be zero. So the fluctuations in the geometry give rise to the odd harmonics.

The event plane method calculates the observed event plane angle directly from the anisotropic flow. It uses the event plane angle to estimate the reaction plane angle.

The event flow vector Q_n is a 2 dimensional vector in the transverse plane. Its components are defined as:

$$Q_{n,x} = \sum_i w_i \cos(n\phi_i) = Q_n \cos(n\Psi_n) \tag{1.3}$$

$$Q_{n,y} = \sum_i w_i \sin(n\phi_i) = Q_n \sin(n\Psi_n) \tag{1.4}$$

In both the equations, the w_i is the weight of particle i and the Ψ_n is the event plane angle. In this research the weight of all particles is set to be 1. The event plane angle is defined as

$$\Psi_n = arctan2(Q_{n,x}, Q_{n,y}) \tag{1.5}$$

The arctan2 is a C language mathematical function. The observed v_n is then calculated using this angle.

$$v_n^{obs}(p_T, y) = \langle \cos(n(\phi_i - \Psi_n)) \rangle \tag{1.6}$$

The brackets mean that the average is calculated over all particles over all events, in a given rapidity and transverse momentum bin for a fixed centrality.

The method used in this research for calculating the anisotropic flow is the two particle correlation. it differs slightly from the event plane method. Instead of using the event plane angle as a correlation, it uses the correlation between 2 particle tracks. The previous equation then becomes:

$$v_n\{2\}^2 = \langle \cos(n(\phi_1 - \phi_2)) \rangle = \langle u_{n,1} u_{n,2}^* \rangle \tag{1.7}$$

In this equation $u_{n,1} = e^{in\phi_1}$, which is the particle's flow vector: $\cos(n\phi_1)$ in the x direction and $\sin(n\phi_1)$ in the y direction.

$$v_n(p_T, y) = \frac{\langle \frac{Q_n}{M} u^*_{n,i}(p_T, y) \rangle}{\sqrt{\langle \frac{Q^a_n}{M_a} \frac{Q^{b*}_n}{M_b} \rangle}} \tag{1.8}$$

Here $u^*_{n,i} = e^{in\phi}$ this is the flow vector of the i^{th} particle. The Q vector is the same Q vector as in the event plane method, only the i^{th} track is taken out in order to prevent auto correlations. The Q^a_n and Q^b_n are the Q vectors of two subsets a and b. All Q vectors are divided by their own multiplicity(M) to remove the multiplicity correlation. It is important that the two subsets are filled by tracks that are not correlated. In order to fill the two subsets without correlating them, the two subset tracks are selected based on:

- Charge
- Pseudorapidity
- Random

For this research the selection is done with the pseudorapidity. The tracks for subsets A and B are selected for positive or negative pseudorapidity values. This choice helps removing close range correlations [16].

Chapter 2

The Large Hadron Collider

The LHC was constructed between 1998 and 2008 by the European Organisation for Nuclear Research (CERN). It consists of two 27km rings. Each ring has 8 straight paths and 8 arcs. The rings cross each other at 4 of the straight paths where the detectors are located.

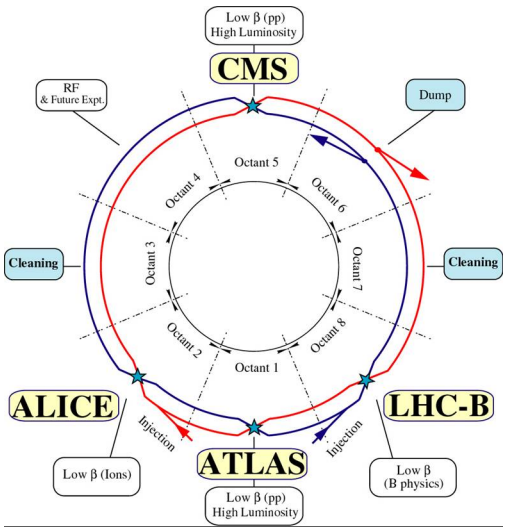

Figure 2.1: Schematic overview of the Large Hadron Collider. [8]

The other 4 straight sections are used to clean up the beam (section 3,7), dumping of used beams (section 6) and for accelerating the beam with the use of radio frequency cavities (section 4). In the sections 8 and 2, the beams are injected from smaller accelerators which first accelerate the beam to 0.999997828 times the speed of light. The LHC was designed to accelerate protons further up to 0.999999991 times the speed of light, which means a collision energy of up to 7 TeV per nucleon, or ions up to 2.76 TeV per nucleon-pair in the case of lead ions. More than 1600 super conducting magnets have been used to control the beam. 1232 dipole magnets have been used to curve the beam inside the ring and 392 quadrupole magnets for the focus of the beam [6]. The goal of the LHC is to test the Standard Model of particle physics, look for new phenomenon at

high energy physics. This includes the search for the Higgs boson and the study of the quark gluon plasma. The LHC has been running from September 2008 until February 2013 with some long and short breaks in between. In February 2013 it was shut down for further improvement and to accelerate to even higher energies than before.

At the LHC there are several detector bases. The two biggest are the Compact Muon Solenoid (CMS) and A Toroidal LHC Apparatus (ATLAS). They are designed for p−p measurements to investigate a wide range of physics. The ATLAS and CMS detector are used to study the same subjects. This includes for the search for the Higgs boson, looking for particles that are candidates for dark matter, studying the CP violation that would explain why there is so little antimatter in the universe and looking for evidence for theories beyond the Standard Model of particle physics. By making different compromises for the design, the two detectors can compliment each other in their search.

Two smaller detectors are the Large Hadron Collidor beauty (LHCb) and A Large Ion Collider Experiment (ALICE). The ALICE detector is designed for heavy ion collisions, in order to study the quark gluon plasma. It will be discussed in greater detail in the next part of this chapter. The LHCb specialises in the detection of beauty quarks. The detector is designed to learn more about the small existing difference between matter and anti matter. Unlike the other detectors, the LHCb does not cover the entire beam pipe. It is focussing on the particles that are pushed forward by collisions along the beam direction, by placing subdetectors behind each other over a range of 20 meters.[10]

2.1 The ALICE experiment

The ALICE collaboration consists of over 1300 physicists, engineers and technicians from more than 36 countries. The ALICE detector [12] is one of the small detectors at the LHC, even though it is still an incredible 16 m high, 16 m wide and 26 m long and it weighs about 10,000 tons. It can be seen in Figure 2.2. The ALICE detector consists of 17 different detectors all designed to measure a specific part of the collision.

The detector can be divided into two major parts of the detector: The main barrel and the muon detector. For this research the ITS, TPC and VZERO detector are mostly used, which is why the focus will be on those rather than the rest of the detectors.

2.1.1 The main barrel

Inside the main barrel there are detectors for measuring hadrons and electrons, the entire main barrel is designed to measure particles with a pseudorapidity range $|\eta| < 0.9$. It is completely around the beam pipe which gives it the ability to measure for the whole azimuthal angle range.

Inner Tracking System

In the centre of the main barrel the Inner Tracking System (ITS) is located. ITS gives information about the p_T spectrum for the low p_T particles. The ITS consists of 6 semi-conductor based detectors. The 6 components are two

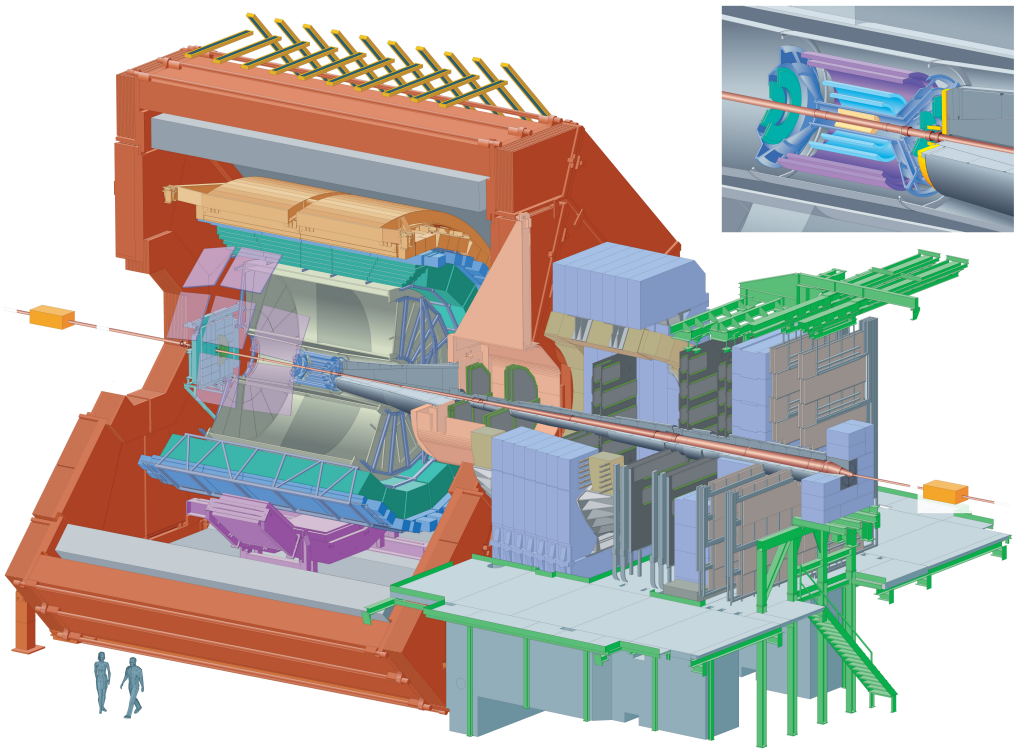

Figure 2.2: The ALICE detector with all of its components. The main barrel is the big red cilinder that covers most of the detectors. Next to the right in blue is the muon detector [2].

Silicon Pixel Detectors(SPD), two Silicon Drift Detectors(SDD) and two Silicone Strip Detectors(SSD). Its main purposes are the determination of the primary and secondary vertices for reconstruction of charm and hyperon decay, particle identification and tracking of low p_T particles and improving the momentum and angle measurements of the TPC.

The two SPDs form the most inner layer of the ITS and they are the only detectors inside the main barrel that have a higher η range ($|\eta| < 1.95$). The reason for this higher range is that the multiplicity can be calculated over a much broader η range so a more accurate measurement can be done for the multiplicity of an event. They are designed to be able to help reconstructing the primary vertices in a high multiplicity environment. The signal from this detector is binary and therefore can not be used for particle identification. The SPDs are made extra thin in order to prevent as much energy loss as possible.

The two SDDs are like gaseous drift detectors, when charged particles go through the silicon, they excite the electrons which will be drifted off to the positive side of the semi conductors on the side. They are used for high precision position data, but also provide information about the energy loss $\frac{dE}{dx}$, which can be used for particle identification. The SSDs use the same technique as the SDDs. [13]

Time Projection Chamber

Around the ITS there is the TPC. It was designed to measure charged particle momentum, particle identification and vertex determination. During heavy ion collisions there a great amount of particles is created, for this a large TPC is needed. The TPC of the ALICE detector can handle a multiplicity up to 20 000 charged tracks. This means that the TPC has to be optimised for both high accuracy and high multiplicity. It has a p_T resolution of 1% for tracks with an momentum below 2 GeV/c and a resolution of 2.5% for tracks up to 4 GeV/c. The TPC is able to separate tracks with a p_T difference of 5 MeV/c. [4] The pseudorapidity range for this detector is $|\eta| < 0.9$ for full track length and with limited track length it can measure up to $|\eta| = 1.5$. The TPC consists of a $90m^3$ barrel with a Ne, CO_2 and N_2 gas mixture that gets ionized by the passing particles. The electrons from the ionized gas are collected at the end of the detector. This is a relatively slow measuring method, but it is needed to provide the accurate data for reconstructing the tracks and energy loss. From the ionisation trails the tracks can be constructed. Through ionization of the gas the particles lose energy. The total energy loss is determined by the amount of ionised electrons that are collected. The energy loss is then used for particle identification.

Transition Radiation Detector

The TRD is designed to distinguish electrons from pions at energies above 1 GeV. The electrons radiate photons in the soft X-ray region when they go through the TRD boundary, while pions do not. Its pseudorapidity range is between $-0.84 < \eta < 0.84$.

Time of Flight

The TOF is located around the TRD where it only measures the time the particle needs to cross the detector. Like the rest of the main barrel it has a pseudorapidity range between $-0.9 < \eta < 0.9$. In the TPC the momentum of the particles was measured. The combination of the TOF and TPC enables the identification of pions kaons and protons.

Electromagnetic Calorimeter

Charged particles are already covered in the previous detectors, but neutral particles are not yet measured. The electromagnetic calorimeter helps reducing the bias in jet quenching studies and it will create a better resolution for the jet energy. Besides that it also improves the ability to measure electrons, neutrons and high momentum photons. It has a pseudorapidity range between $-0.7 < \eta < 0.7$

High Momentum Particle Identification

To measure high momentum particles a new method is needed, while the ITS and TPC make use of energy loss to calculate what kind of particles there were, the HMPID makes use of Cherenkov radiation for its calculations. When high momentum particles go through the detector they will emit photons because

their speed is higher than the speed of light in that medium. The emitted photons are detected by photon counters inside the detector. The detector has a pseudorapidity range between $-0.6 < \eta < 0.6$

Photon detectors

The photon spectrometer (PHOS) is used to measure the photons in a large p_T range (0.5-10 GeV/c). The pseudorapidity ranges between $-0.12 < \eta < 0.12$. The other photon detector is the photon multiplicity detector (PMD), which measures the multiplicity of the photons before any showers occur. PMD has a pseudorapidity between $1.8 < \eta < 2.6$ The two photon detectors are combined to account for all aspects of the photons. The PHOS is a very accurate photon detector, it only has a small region in which it measures. The PMD observes in a very large region but is less accurate in the measurements.

ALICE Cosmic Ray Detector

The cosmic radiation detector is, unlike the others, not focused on what happens on the inside of the ALICE detector. It is put outside of the main barrel for measuring the incoming cosmic radiation. The calibration was done before they started using the LHC. Since there were no beams colliding yet during that time it was the perfect opportunity to get a good background calibration, and also to test how well the other individual detectors were in alignment with each other.

2.1.2 Muon spectrometer

Outside the main barrel the muon spectrometer is located. It measures muon pairs that are created by decaying quark-antiquark pairs, mainly charm-anticharm and bottom-antibottom pairs. The pseudorapidity of the muon spectrometer is between $2.5 < \eta < 4.0$ The muon spectrometer is mostly used for low p_T quark-antiquark particles because at higher energies the decay will not be in muons, but in B decay.

Zero Degree Calorimeter

The Zero Degree Calorimeters (ZDCs) are located 116 m away in the z direction at both sides of the ALICE detector, at a pseudorapidity range between $4.8 < \eta < 5.7$. They are used after the collisions happened, they separate the left overs of the collision into 3 groups, the positive, negative en neutral particles. The first group will consist of the protons that are still left, the second group is used as a calibration since there are supposed to be only protons and neutrons left. The last group consists of the left over neutrons. By collection all the debris it can be calculated how many neutrons/protons were used in the collisions.

Forward Multiplicity Detector

Together the ZDCs, VZERO and the FMD make up for the small angle detectors or forward detectors. the FMD is designed to measure the small angle particles that are created at the collisions. For this it uses pseudorapidity ranges from $-3.4 < \eta < -1.7$ and $1.7 < \eta < 5.0$. Besides calculating all the particles that

were created at the collision it also studies the elliptic flow, the phase transition to the QGP and fluctuations in the multiplicity.

VZERO detector

The VZERO detector is the last of the forward detectors. The VZERO detectors are designed to estimate the centrality of collisions and to work as a trigger system for the rest of the detector. It consists of 2 arrays of scintillator counters, named VZEROA and VZEROC, their pseudorapidity ranges $2.8 < \eta < 5.1$ and $-3.7 < \eta < -1.7$ respectively. Both of these are made out of 4 rings all divided into 8 segments of 45 degree. The detector is triggered when there is enough energy deposited onto it. This energy gives an estimate for the centrality of the collision.

Chapter 3

Results

The data was collected in November - December 2010 during the first heavy ion run. Before the elliptic flow and higher order flows are shown, the cuts made on the events and tracks will be discussed.

3.1 Event selection

Only a small sample of the data is used in this analysis (200 000 events). They are first selected on their centrality. In order to get good results, bad events have to be removed. This is done by making a centrality cut for all the events. There are three centrality estimators: the VZERO multiplicity, the second is the track multiplicity and the last one is the tracklet multiplicity coming for the ITS detector. A Glauber model is run over these multiplicities to convert the multiplicities into a centrality percentage. The difference between the VZERO and track centrality estimator of a single event can only be less than 5%. The centrality cut is $|C_{VZERO} - C_{track}| < 5\%$.

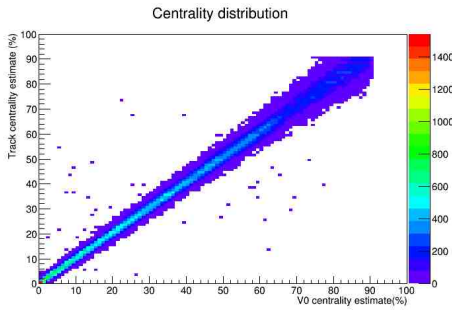

Figure 3.1: The centrality distribution before the cut. There are events still present with very different percentages for the centrality.

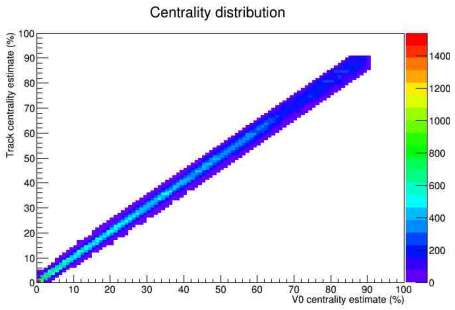

Figure 3.2: The centrality distribution after the cuts were applied. All events where the difference between the two estimators differed too much were removed.

In this research the VZERO centrality estimator is used as the standard centrality selector. The other two are merely used to quantify the systematic

error for the centrality parameter. For the anisotropic flow coefficients, the events were put into 6 centrality bins: (0-5%,5-10%,10-20%,20-30%,30-40%,40-50%) to be used for calculations. The centrality cut has also an effect on the multiplicity of the events. The multiplicity before and after the cut show that all the events with a multiplicity that does not fit with the model are removed. Their results can be seen in Figures 3.3 and 3.4. In the figures it can be seen that the distribution is very smooth after the cut compared to before the cut.

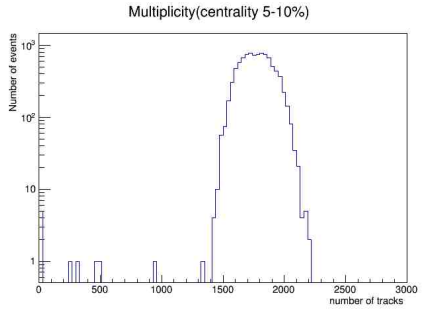

Figure 3.3: The multiplicity distribution before the cut. There are still some events present that have a multiplicity that is not expected in this centrality bin.

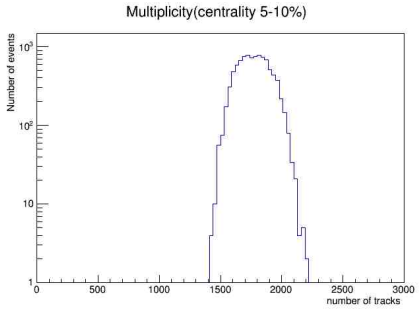

Figure 3.4: The multiplicity distribution after the cut. The distribution is cleaned up for bad events.

Besides the centrality cut, there is also a cut made for the reconstructed vertex. The point of interaction for the collision is constructed by tracking all particles. This constructed point of interaction is called the reconstructed vertex. The reconstructed vertex is measured along the beam direction (z axis). If the reconstructed vertex is more than 10 cm from the centre in the z axis the event will not be accepted. In Figures 3.5 and 3.6 the result from the cut is visible.

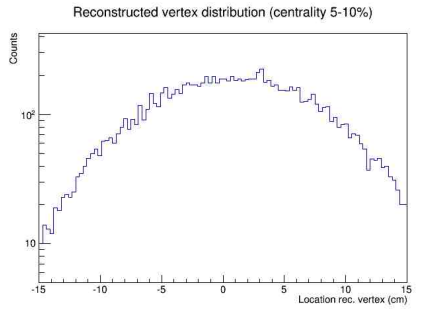

Figure 3.5: The reconstructed vertex distribution before the cut. It runs up till 15 cm away from the centre.

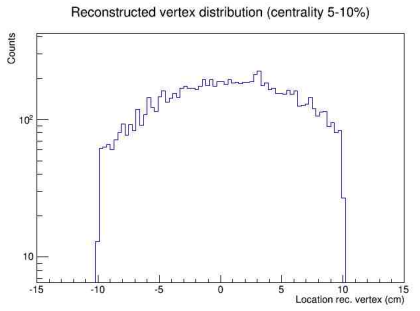

Figure 3.6: The reconstructed vertex distribution after the cut. Now only events within 10 cm of the centre are accepted for the calculations.

3.2 Track selection

Once the event selection is done, there are several cuts made on the tracks of every event. The transverse momentum is set between 0.2 and 6 GeV/c for all the calculations. The reason why the minimum p_T is at 0.2 and not at 0 is because of the magnetic field inside of the detector. With a low momentum the magnet bends the released particles too much, which causes them to create a spiral instead of creating a small curvature through the detector. Because of this they cannot be measured accurately. The reason the particles are cut above 6 GeV/c is the lack of high p_T tracks. There are too few particles with a transverse momentum of more than 6 GeV/c in the data provided to give good statistics.

The pseudorapidity (η) is a coordinate which is used to describe the angle between a particle and the beam axis.

$$\eta = \ln(\tan(\frac{\theta}{2})), \tag{3.1}$$

at which θ the angle is between the particle's momentum and the beam axis. If a particle has an angle of 90 degrees with the beam axis it would give an η of 0. At an angle of 0 degrees, η would go to infinity. Because of the symmetry around $\theta = 90$ degrees, both positive and negative η are used. For this research the pseudorapidity selection allows only tracks with a η between -0.8 and 0.8. This is done because between 0.8 and 0.9 pseudorapidity there occur edge problems. At that pseudorapidity range you lose full tracks.

Particles that go through the TPC deposit energy onto it. The TPC measures this as a mean energy deposit, denoted as $\frac{dE}{dx}$. The mean energy deposit is selected for $\frac{dE}{dx} > 10$. This selection is done in order to remove laser tracks that are used for calibration during the run.

Tracks are extrapolated from the signals given by the detectors. With the use of the Distance of Closest Approach (DCA) they are selected for good tracks. The DCA is the extrapolated distance from the measured track to the primary vertex of the collision. The DCA runs both in the xy field and in the z direction. For both DCAs the distance is set in cm. The tracks are selected if they have a DCA < 3 cm for both directions.

The next parameter is the number of TPC clusters (ncl). When a charged particle enters the TPC it will induce a signal through the detector. When the charge passes the threshold value it will be labelled as a cluster. The maximum amount of clusters for one track is limited to 159, because this is the total number of pad rows inside a TPC section. In this research the tracks that have an ncl > 70 are selected for the calculations.

These track cuts, together with the event cuts, must assure a good track selection for the anisotropic flow calculations. The standard track cuts are shown in Table 3.1.

3.3 Elliptic flow

The method for calculating the elliptic flow was already discussed in Chapter 1. The v_2 values are calculated per centrality bin and plotted against their p_T value in Figure 3.7.

Parameter	Cuts
transverse momentum	$0.2 < p_T < 6$ GeV/c
pseudorapidity	$\|\eta\| < 0.8$
number TPC clusters	ncl > 70
reconstructed vertex	vertex < 10 cm
$DCA_{x,y}$	dcaxy < 3 cm
DCA_z	dcaz < 3 cm

Table 3.1: The standard track cuts for the parameters used in this research. If a track does not meet all of these requirements it is removed.

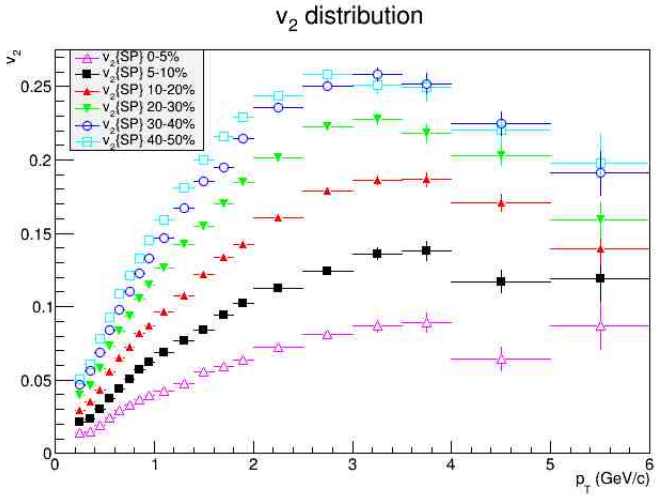

Figure 3.7: The elliptic flow for every centrality bin set against their p_T value.

Between a p_T of 0.2 and 3 GeV/c the elliptic flow is increasing with p_T and after 3 GeV/c decreasing with p_T. There is a strong centrality dependence visible for the elliptic flow.

The elliptic flow is given a correction for the non uniform ϕ distribution. To correct for this non uniform distribution, the average $cos(\phi_1 - \phi_2)$ was calculated and subtracted for the calculation by using:

$$\langle cos(\phi_1 - \phi_2)\rangle = \langle \cos(\phi_1)\cos(\phi_2) + \sin(\phi_1)\sin(\phi_2)\rangle \tag{3.2}$$

$$\langle \cos(\phi_1)\cos(\phi_2) + \sin(\phi_1)\sin(\phi_2)\rangle = \langle\cos(\phi_1)\rangle\langle\cos(\phi_2)\rangle + \langle\sin(\phi_1)\rangle\langle\sin(\phi_2)\rangle \tag{3.3}$$

As the two $\phi_{1,2}$ are coming from charged particles, they can be combined into:

$$\langle\cos(\phi_1)\rangle\langle\cos(\phi_2)\rangle + \langle\sin(\phi_1)\rangle\langle\sin(\phi_2)\rangle = \langle\cos(\phi_1)\rangle^2 + \langle\sin(\phi_1)\rangle^2 \tag{3.4}$$

When subtracting this from the flow coefficients, the result is:

$$v_n(p_T, y) = \frac{\langle \frac{Q_n}{M} u^*_{n,i}(p_T, y)\rangle - \langle\cos(\phi_1)\rangle^2 - \langle\sin(\phi_1)\rangle^2}{2\sqrt{\langle \frac{Q_n^A}{M_A}\frac{Q_n^{B*}}{M_B}\rangle - \langle\cos(\phi_A)\rangle\langle\cos(\phi_B)\rangle - \langle\sin(\phi_A)\rangle\langle\sin(\phi_B)\rangle}} \tag{3.5}$$

In Equation 3.5, the correction is also applied to the used weight, but here the last step in Equation 3.4 cannot be made because in this case the $\phi_{A,B}$ run over their own subsets A and B who are mentioned in Section 1.2.1. This corrected result compared to the original elliptic flow is plotted in Figure 3.8 for the centrality bins 0-5%, 10-20% and 40-50%. In the figure it can be seen that the results do not change a lot after the correction. The ϕ distribution is almost completely flat.

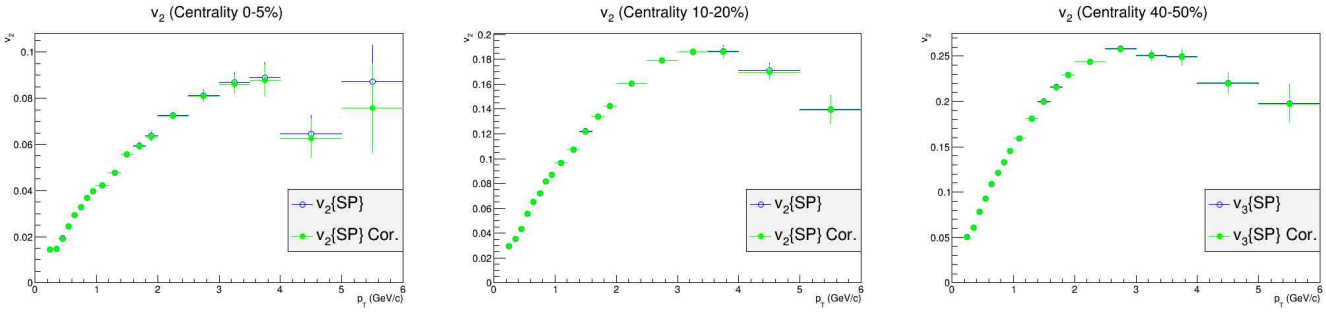

Figure 3.8: The correction for the non uniform ϕ distribution for the centrality bins 0-5%,10-20%,40-50%.

3.3.1 Systematic error

The standard cuts were varied in order to see what the influence is of a certain parameter on the anisotropic flow. These changed cuts are used to calculate a ratio between the standard cut and the changed cut. This ratio is used to see the influence of a single parameter on the result. The way the cuts were selected was by looking for sensible differences. If the cuts were too small, the changes would not have been visible. If, on the other hand, too many tracks are lost due the cut, the statistic won't be reliable any more to give a good result. The cut therefore has to be significant enough to see if the parameter influences the results in an odd way, but not too high to prevent too much loss of statistics.

Besides using these cuts for the systematic error, they are also used to see if there are any odd things going on in the programs that are used to calculate the v_n's. Cuts made on the pseudorapidity for example should have no influence on the p_T distribution as they are not correlated. If it does look correlated, there could be something wrong with the data processing.

For these additional cuts the following parameters are used: η, rec. z vertex, ncl, DCA_{xy}, DCA_z, charge and centrality. The charge parameter is done different than the rest of the parameters. To calculate the ratios for the charge parameter, the tracks are selected for either positive or negative charge. After the cut the selected tracks are used to calculate the anisotropic flow the same way as was done before. An example for a charge cut ratio can be seen in Figure 3.9

By taking the average of the graph, the ratio can be calculated per centrality bin. The ratio is made for all centralities for both cuts of positive and negative tracks. The ratio that differs the most from the original is selected per centrality bin as the systematic error of that parameter. The contribution to

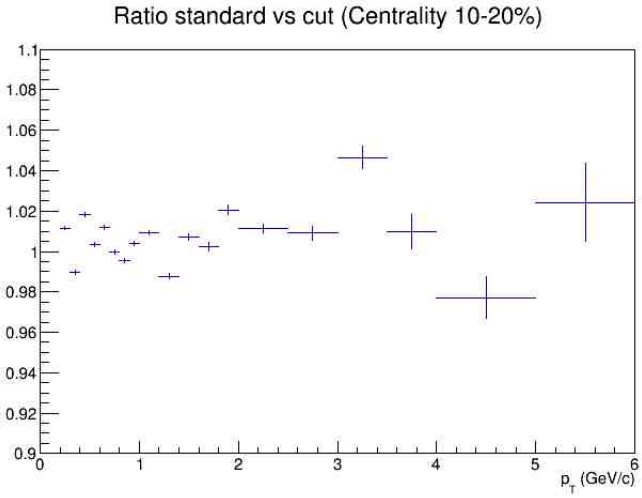

Figure 3.9: The ratio between the elliptic flow with just negative tracks and all tracks. Centrality bin is 10-20%.

the systematic error is the difference between the ratio and 1. For the other parameters the standard cut is varied and the calculation for the elliptic flow is done again. The ratio is taken between the two elliptic flows and it is used to calculate the total systematic error, which is calculated by,

$$\sigma_{syst} = \sqrt{\sigma^2_{cent} + \sigma^2_{zvtx} + \sigma^2_{ncl} + \sigma^2_{dcaxy} + ...} \tag{3.6}$$

The additional cuts made on the rest of the parameters are shown in Table 3.2

Parameter	Additional cuts
Centrality	Track and tracklet multiplicity
pseudorapidity	<0.6
number TPC clusters	>60, >80
reconstructed vertex	<7
DCA_{xy}	<1, <0.5
DCA_z	<1, <0.5

Table 3.2: The cuts that are used for the calculation of the systematic error per parameter. The centrality cut represents a different centrality estimator as selector. The standard is the VZERO multiplicity.

The ratios were made for all the cuts for every centrality. The largest ratios were all at the 0-5% centrality bin. The resulting systematic errors are shown in Table 3.3. The systematic error seems to decrease as the collisions get more peripheral.

To implement the systematic error, the elliptic flow is multiplied by the total systematic error and shown in Figure 3.10. The DCAs and the charge

Parameter	Syst. error(%) Cent. 0-5%	Cent. 5-10%	Cent. 10-20%	Cent. 20-30%	Cent. 30-40%	Cent. 40-50%
Centrality	0.7	0.5	0.4	0.4	0.2	0.6
pseudorapidity	1.7	1.1	0.9	0.7	0.4	0.2
number TPC clusters	1.0	0.6	0.2	0.1	0.2	0.2
reconstructed vertex	1.2	0.5	0.1	0.1	0.1	0.1
DCA_{xy}	1.6	1.5	0.6	0.3	0.5	0.5
DCA_z	1.9	1.2	0.5	0.3	0.5	0.3
Charge	1.6	0.9	0.5	0.3	0.7	0.6
Total error	3.8	2.56	1.0	1.0	1.1	1.1

Table 3.3: The systematic error of the individual parameters and the total error. For every centrality bin the systematic error is calculated here.

parameters provide the highest systematic error overall. The elliptic flow is also compared to other results. The comparison results for the differential elliptic flow used the two particle cumulant method instead of the two particle scalar product method as was used in this research [5]. The results come from the ALICE preliminary results.

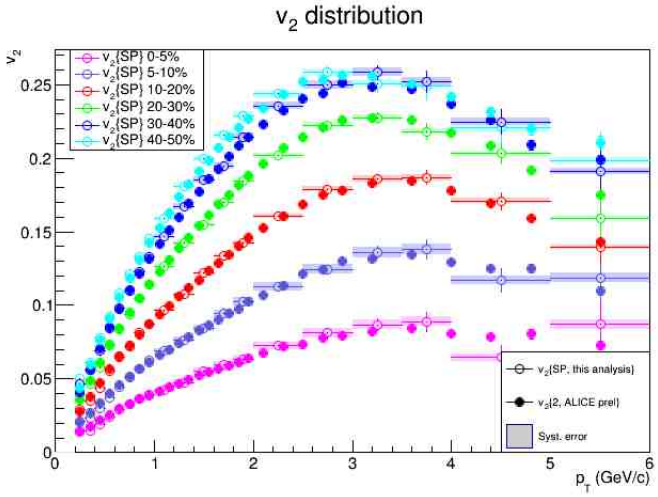

Figure 3.10: The elliptic flow with systematic error implemented. The results of this research are also set against the comparison data. [5]

In Figure 3.10 the elliptic flow is compared to the ALICE preliminary results [5]. The results are in good agreement between this analysis and the two particle method for the investigated p_T range and all the centrality bins.

3.4 Triangular flow

For the triangular flow the results are calculated in the same way as for the elliptic flow. Figure 3.11 shows that the triangular flow is slightly lower than

the elliptic flow for all centrality bins except for 0-5%. Between 0.2 and 3 GeV/c the triangular flow increases with p_T. It also shows a small decrease with p_T after 3 GeV/c. Unlike the elliptical flow the triangular flow does not show a strong centrality dependence. Because the triangular flow is non zero, there seems to be fluctuations in the geometry of the collision.

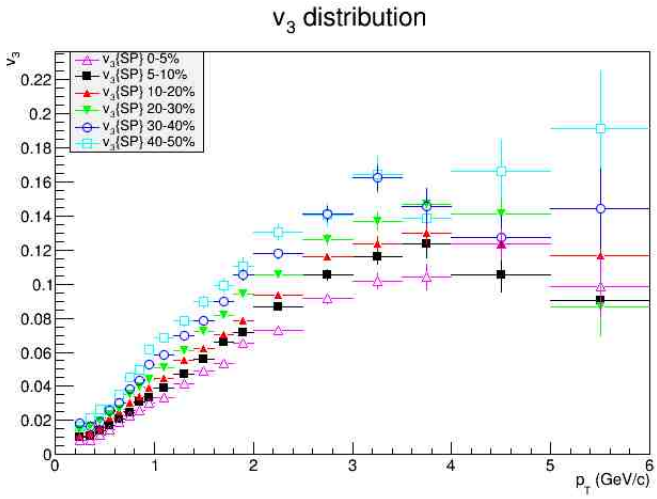

Figure 3.11: The triangular for every centrality set against their p_T value.

The same correction that was done on the elliptic flow is applied to the triangular flow. The correction to the triangular flow shows no real changes, except at the highest p_T bin in the 40-50% centrality bin. Here the change is almost larger than the error bars of the value.

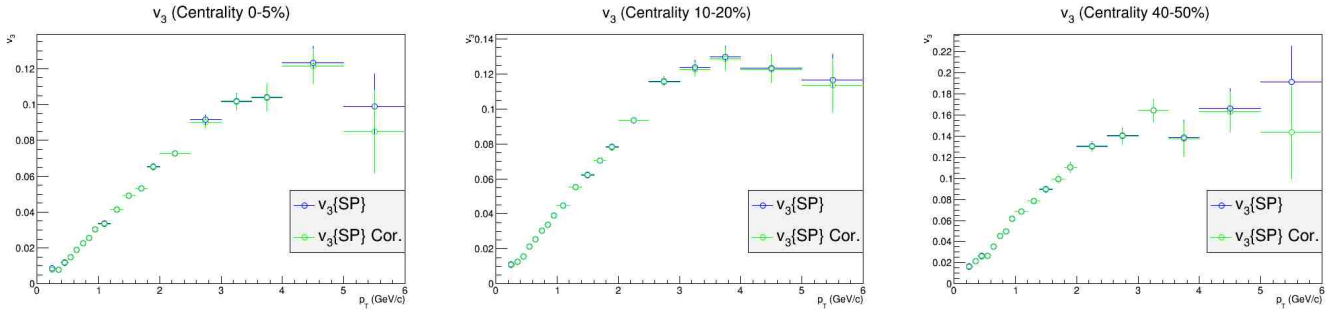

Figure 3.12: The correction for the triangular flow for the non uniform ϕ distribution for the centrality bins 0-5%,10-20%,40-50%.

3.4.1 Systematic error

The systematic error for the triangular flow is calculated in the same way as the elliptic flow. For this systematic error the charge parameter was not used due to strange results with just positive or negative tracks. The resulting systematic errors per centrality bin can be seen in Table 3.4.

Centrality bin	Systematic error (%)
0-5%	6.0
5-10%	5.7
10-20%	2.9
20-30%	2.7
30-40%	1.5
40-50%	2.8

Table 3.4: The total systematic error per centrality bin. In this result the charge parameter is not included.

The systematic error is considerably higher for the triangular flow than for the elliptic flow. The highest systematic error is for the triangular flow in the 0-5% bin, this is the same centrality bin as the highest systematic error for the elliptic flow.

3.5 Integrated flow

The anisotropic flow discussed above is referred to as the differentiated flow. In addition to the differentiated flow there is also the integrated flow. This is made by integrating the previously calculated anisotropic flow coefficients. The integrated flow is calculated as follows:

$$v_n^{int} = \frac{\sum_i v_n^i \, p_T}{\sum_i p_T^i}, \tag{3.7}$$

where the summation is done per centrality bin over all p_T bins. The error for the integrated flow is:

$$\sigma_{v_n^{int}} = \frac{\sqrt{\sum_i \sigma_{v_n^i}^2 \, p_T^{i2}}}{\sum_i p_T^i} \tag{3.8}$$

In this equation, the $\sigma_{v_n^i}$ is the error in the flow values and the p_T is the transverse momentum again. The integrated flow is not set against the p_T value, but is set against their centrality instead.

The results for the integrated elliptic flow are shown in Figure 3.13 compared to the ALICE preliminary results [14]. The systematic error was calculated per centrality bin and is therefore also implemented in the integrated flow.

The results from the ALICE preliminary results give a lower value than this analysis. The triangular flow was also integrated in the same way the elliptic flow was. For the integrated triangular flow there was no data set to compare it with. The result is shown in Figure 3.14. The integrated triangular flow increases with centrality between 0 and 60% centrality. The values for the integrated triangular flow are much lower than those of the integrated elliptic flow.

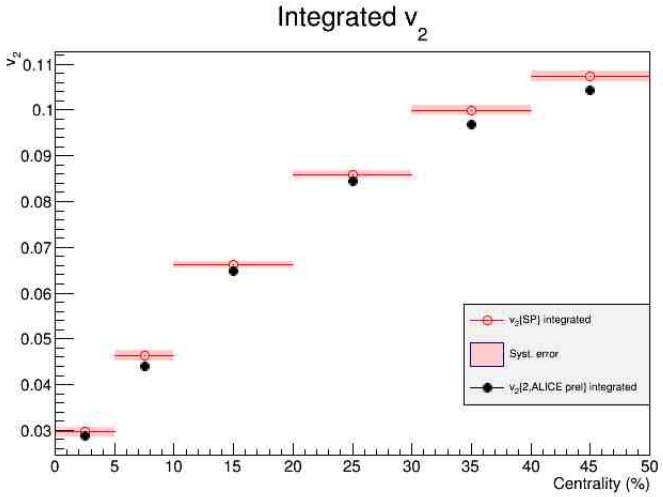

Figure 3.13: The integrated elliptic flow. Compared to the ALICE preliminary results [14].The systematic error is also included in this figure.

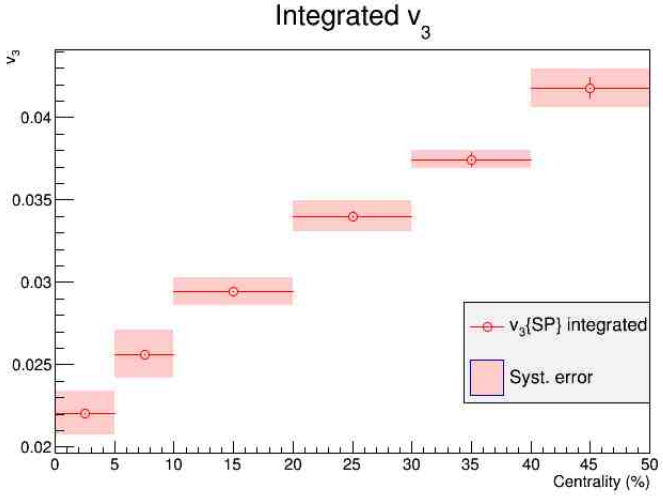

Figure 3.14: The integrated triangular flow with systematic errors included.

Chapter 4

Discussion

4.1 Elliptic and triangular flow

The results from this analysis and the compared results are in good agreement with each other at all but the highest p_T range. It is at these ranges that the results from this analysis start to differ from the comparing data. But within their statistical errors, also the highest p_T bins are in agreement with the compared results. At the highest p_T range there are less tracks than at the lowest p_T range. Less particles at high momentum result in less accurate anisotropic flow values. It also results in larger error bars as the transverse momentum increases.

The triangular flow is lower than the elliptic flow at all but one centrality bin. At a centrality of 0-5% the triangular flow has a higher peak. The two show a lot of resemblances in their structure. Both of them have an increase between 0.2 and 3 GeV/c and the maximum values are around 3 GeV/c. The centrality dependence of the elliptic flow is much higher than the triangular flow. Considering that the elliptic flow is caused by the pressure gradient of the almond shape of the collision and the triangular flow is caused by fluctuations in this shape, this is the expected result. A smaller almond shape would give a higher pressure gradient resulting in a larger elliptic flow, while the fluctuations do not necessary have to become larger for higher centrality percentages.

The additional correction for the non uniform distribution of the azimuthal angle has shown to be very small. The difference between the corrected and not corrected anisotropic flow is small enough to be neglected in this research.

In this research the VZERO multiplicity is used for the calculation of the elliptic flow. By picking the track multiplicity in the TPC detector instead of the VZERO, the results did not change much as was visible in the small systematic error for this parameter. The same goes for the tracklet multiplicity. From this there can be concluded that there is no preferred centrality estimator for better results.

The systematic error is for both the elliptic flow and triangular flow higher at less peripheral collisions. The results show that the systematic error for the triangular flow is significantly higher than the elliptic flow, even without the systematic error of the charge parameter. If that parameter is included as well the systematic error will increase even more. For this research the charge

parameter was not included in the systematic error calculation of the triangular flow because there seemed to be a problem with the data analysis. With more time for this research, this could be checked and the data can be corrected for this.

The integrated flow shows a clear rise towards the peripheral collisions. For both the elliptic and triangular flow. This is expected when comparing them to the differential elliptic and triangular flow. The integrated elliptic flow is higher than the triangular flow. Even at the 0-5% centrality bin, where the triangular flow has a higher peak.

4.2 Future improvements

There are a lot of options to improve these calculations. The start would be to use more events as it seemed that at high p_T the statistical errors were getting really high. At low p_T, where there were a lot of tracks, the results were in good agreement with the comparison data, therefore more tracks will help improving the accuracy of the anisotropic flow for high p_T. With more data available it is also possible to expand the p_T range to see what happens with the elliptic and triangular flow for higher momentum. There seems to be a small decrease after 3 GeV/c but especially for the triangular flow the 40-50% centrality bin seems to keep on increasing. It is expected to go down as the other bins since they are all are decreasing and the odd result could just be caused by the lack of tracks, but there might be something going on there. A higher p_T range can give good insight into the actual development for the anisotropic flow at high p_T, where for now only extrapolations can be made. For the same reason higher centrality bins can give more insight in the development of the peripheral collisions.

Besides using more events there is the option to use a different method for the calculation of the elliptic flow. The two particle cumulant method calculated the anisotropic flows directly between each set of particles. This method can also be expanded to more than two particles which allows it to remove even more non-flow effects [16].

The results are only compared to the ALICE preliminary results, but also theoretical models can be used as a comparison to the results.

Even though re-scattering inside the quark gluon plasma is the most used explanation for anisotropic flow, there are also other effects that can cause anisotropic distributions. The partonic structure of the colliding nuclei or direct anisotropy in particle emission from color glass condensates can both be responsible for anisotropic flows [16]. These subjects can also be studied to see their contribution to the anisotropic flow.

Appendix A

The coordinate system

In the ALICE detector a special coordinate system is used. It is based around the beam direction. The x axis is defined to be perpendicular to the beam direction and is directed to the middle of the LHC ring. The y axis is perpendicular to the beam direction as well, but stands vertically up in the air. The z axis is defined to be parallel to the beam direction with the positive value in the counter clock wise direction. The two angles are defined with the use of the x,y,z. The azimuthal angle ϕ is in the xy plane. In the positive x direction (pointing to the inside of the detector) the angle is 0, in the y direction the angle is $\pi/2$ and at negative x it is π. The polar angle is from the z axis toward the xy plane, with a value of $\pi/2$ in the xy plane and π in the negative z direction. [4]

Bibliography

[1] A. Bilanzic, *Anisotropic Flow Measurements in ALICE at the Large Hadron Collider*, (2012)

[2] A Large Ion Collider Experiment, CERN, 25 May 2013

`http://aliceinfo.cern.ch/Public/en/Chapter2/Chap2Experiment-en.html`

[3] O.S. Bruning *et al.*, *LHC Design Report Volume I*, (2004)

[4] A. Dobrin, *R-hadron Searches and Charged Pion Spectra at High Transverse Momentum in Proton-Proton Collisions at the LHC using the ALICE Detector*, (September, 2010)

[5] A. Dobrin, *Elliptic flow of charged particles in Pb-Pb collisions at* $\sqrt{s_{NN}} = 2.76$ *with the ALICE experiment*, (July,2011), arXiv:1107.0454v1 [nucl-ex]

[6] L. Evans and P. Bryant, *LHC Machine*, (2008), JINST 3 S08001

[7] The history of CERN, CERN, 30 May 2013,

`http://timeline.web.cern.ch/timelines/the-history-of-cern/overlay#1986-06-10%2023:15:00`

[8] LHC Machine Outreach, CERN, 25 May 2013,

`http://lhc-machine-outreach.web.cern.ch/lhc-machine-outreach/images/lhc-schematic.jpg`

[9] B. Muller, *The "perfect" fluid quenches jets almost perfectly*, Progress in Particle and Nuclear Physics, p. 551-555, (April, 2009)

[10] M.Riordan and W.A.Zajc, *The first few micro-seconds*, Scientific American 294 (2006) 24.

[11] R. Snellings, *Elliptic flow: a brief review*, New J. Phys. 13 (2011) 055008 doi:10.1088/1367-2630/13/5/055008

[12] The ALICE Collaboration, *Technical proposal for A Large Ion Collider Experiment at the CERN LHC*, (Cern, Geneva, 1995).

[13] The ALICE Collaboration, *ALICE Inner Tracking System (ITS): Technical Design Report*, (CERN, Geneva, 1999)

[14] The ALICE Collaboration, *Elliptic flow of charged particles in Pb-Pb collisions at* $\sqrt{s_{NN}} = 2.76$ Phys. Rev. Lett. **105**, 252302 (2010).

[15] S.A. Voloshin, Y. Zhang, *Flow study in relativistic nuclear collisions by Fourier expansion of Azimuthal particle distributions*, Z.Phys. C70 (1996) 665-672

[16] S.A. Voloshin, A.M. Poskanzer and R. Snellings, *Collective phe-nomena in non-central nuclear collisions*, (October 2008)